Am J Clin Exp Urol 2026;14(5):204-214
www.ajceu.us /ISSN:2330-1910/AJCEU0174390

Original Article

Integrative analysis reveals C3 downregulation associated with promoter methylation and immune context in prostate cancer

Kanako Matsuoka[1,4], Qinghua Fang[1], Tanveer Ahmed Mohammed[1], Mohammad Reza Askarpour[1], Hong Luo[1], Jianhua Zhou[1], Yoshiyuki Kojima[4], Naoki Yoshimura[1,3], Zhou Wang[1,2,3]

[1]Department of Urology, University of Pittsburgh School of Medicine, Pittsburgh, PA 15232, USA; [2]UPMC Hillman Cancer Center, University of Pittsburgh School of Medicine, Pittsburgh, PA 15232, USA; [3]Department of Pharmacology and Chemical Biology, University of Pittsburgh School of Medicine, Pittsburgh, PA 15213, USA; [4]Department of Urology, Fukushima Medical University School of Medicine, Fukushima 960-1295, Japan

Received May 30, 2026; Accepted September 2, 2026; Epub October 25, 2026; Published October 30, 2026

Abstract: Objective: The complement system is increasingly recognized as a regulator of the tumor microenvironment. However, its role in prostate cancer progression and immune infiltration remains unclear. This study aimed to clarify complement gene expression patterns in prostate cancer and immune infiltration, particularly complement component 3 (C3) expression and its promoter methylation. Methods: Transcriptomic and DNA methylation data from The Cancer Genome Atlas prostate adenocarcinoma (TCGA-PRAD) cohort and GSE21032 were analyzed. Complement gene expression was compared among adjacent normal, primary tumor, and metastatic samples. Associations between gene expression, promoter methylation, and immune infiltration were evaluated using correlation and multivariable linear regression analyses. Gene Set Enrichment Analysis was performed for C3-associated pathways. C3 expression was examined in prostate cell lines by quantitative PCR and Western blotting. Results: Multiple complement components showed differential expression across disease states. In TCGA-PRAD, C2 and C4A were upregulated in primary tumors compared with adjacent normal tissues (both $P < 0.001$), whereas C3 and C7 were downregulated ($P = 0.025$ and $P < 0.001$, respectively). In GSE21032, stage-based analysis showed further reduction of C3 and C7 in metastatic lesions ($P = 0.002$ and $P < 0.001$, respectively). In multivariable analysis, both C3 promoter methylation and immune infiltration score were independently associated with C3 expression ($P = 0.002$ and $P < 0.001$, respectively). In contrast, C7 was associated with immune infiltration and tumor status but not promoter methylation. Low C3 expression was associated with enrichment of MYC target and androgen response pathways. C3 expression was reduced in prostate cancer cell lines at both the mRNA and protein levels. Conclusion: Our findings indicate that C3 is reduced in prostate cancer and is associated with promoter methylation, immune context, and proliferative signaling pathways. These findings suggest that C3 downregulation may be a distinct feature of complement alteration during prostate cancer progression.

Keywords: Prostate cancer, complement components, complement component 3, promoter methylation, immune infiltration

Introduction

Prostate cancer represents one of the most commonly diagnosed malignancies in men worldwide, with 1.4 million new cases diagnosed annually [1]. Although localized prostate cancer often shows favorable outcomes following curative interventions, the clinical prognosis becomes increasingly poor upon progression to metastatic or castration-resistant prostate cancer (CRPC) [2]. CRPC usually develops when recurrent or metastatic prostate cancer progresses despite androgen deprivation therapy. Persistent androgen receptor signaling is a central mechanism of castration resistance [3], with additional contributions from epigenetic dysregulation and changes in the tumor microenvironment (TME) [4, 5]. TME is increasingly recognized as an important contributor to cancer progression. In prostate cancer, the tumor is often characterized by an immunologically cold phenotype, with limited T-cell infiltration and poor responsiveness to immunotherapy [4]. However, the molecular

https://doi.org/10.62347/KORS7891

mechanisms underlying this immune-evasive phenotype remain poorly understood, particularly regarding the contribution of the complement system, a key component of innate immunity [6-8].

Complement activation has been associated with both anti-tumor immune responses and tumor-promoting inflammation, depending on the biological context [7, 8]. Complement component 3 (C3) is the central component of the complement cascade and generates effector fragments involved in inflammation and immune regulation. In prostate cancer, complement-related alterations have been reported, including early complement activation and increased expression of complement receptors such as C3aR and C5aR in tumor tissues [9, 10]. However, the expression pattern of C3 across prostate cancer states and the regulatory mechanisms underlying C3 dysregulation remain unclear. Promoter DNA methylation is a well-established mechanism of gene silencing in prostate cancer [11], and glutathione S-transferase pi 1 (GSTP1) promoter hypermethylation is one of the most characteristic features [12, 13]. We therefore incorporated DNA methylation data into our integrative analysis to assess its potential contribution to complement component expression.

We performed an integrative analysis of transcriptomic and DNA methylation data from The Cancer Genome Atlas prostate adenocarcinoma (TCGA-PRAD) cohort and an independent dataset (GSE21032) to clarify the expression patterns and potential epigenetic regulation of complement components in prostate cancer. Complement component expression was examined across normal, primary, and metastatic samples, and the relationship between C3 expression, promoter methylation, and immune context was assessed primarily in TCGA-PRAD. In addition, we examined whether C3 expression was altered in prostate cancer cell lines as compared to non-malignant prostatic cell lines.

Materials and methods

Data sources

Transcriptomic data and sample annotations for prostate adenocarcinoma were obtained from TCGA via the University of California Santa Cruz (UCSC) Xena platform [14, 15]. Gene expression profiles (TCGA.PRAD.sampleMap/HiSeqV2) included 497 primary tumor samples, 52 adjacent normal prostate tissues, and one metastatic sample. The single metastatic sample was excluded, and primary tumor and adjacent normal samples were used for the TCGA normal-versus-tumor comparison. Gene expression values were derived from RNA-Seq data using Expectation-Maximization (RSEM)-normalized expected counts and transformed using log2(x+1) [16].

DNA methylation data for TCGA-PRAD were also obtained from the UCSC Xena platform (Illumina HumanMethylation450) [15]. Beta values (β), representing the proportion of methylation at each CpG site, were used for downstream analyses. Promoter-associated CpG probes were defined as those annotated to TSS1500, TSS200, 1stExon, or 5'UTR regions according to the Illumina HumanMethylation450k annotation (hg19) [17]. For each gene, the mean promoter β value was calculated by averaging all annotated promoter CpG probes. Methylation and expression data were matched using TCGA sample barcodes.

To examine complement expression patterns across disease stages, we also used the GSE21032 dataset from the National Center for Biotechnology Information (NCBI) Gene Expression Omnibus (GEO), which includes 29 adjacent normal tissues, 131 primary tumors, and 19 metastatic lesions [18]. Raw CEL files were processed using the Robust Multi-Array Average (RMA) algorithm [19], including background correction, quantile normalization, and log2 transformation. For multi-subunit complement components such as C1 (C1QA, C1QB, and C1QC) and C8 (C8A, C8B, and C8G), the mean expression of their respective subunits was used to represent the complex. For C4, C4A was analyzed as the representative gene based on probe availability in the dataset.

Cell culture

LNCaP cells were obtained from the American Type Culture Collection (ATCC, Manassas, VA, USA). C4-2 cells were originally obtained from Dr. Leland W. K. Chung (Cedars-Sinai Medical Center, Los Angeles, CA, USA), as previously described [20]. The benign prostatic epithelial cell line BHPrE1 and the immortalized benign

prostatic epithelial cell line BPH-1 were derived from laboratory stocks originally obtained from Dr. Simon Hayward at NorthShore University HealthSystem (Evanston, IL, USA), as previously described [21]. Cells were cultured at 37°C in a humidified atmosphere containing 5% CO_2. LNCaP, C4-2, and BPH-1 cells were maintained in RPMI 1640 (Corning, Corning, NY, USA; catalog no. 11875093) supplemented with 10% fetal bovine serum (FBS; Atlanta Biologicals, GA, USA; catalog no. 900-108), 1% penicillin-streptomycin (10,000 U/mL; Gibco, Thermo Fisher Scientific, Waltham, MA, USA; catalog no. 1540122), and 1% L-glutamine (200 mM; Gibco, Thermo Fisher Scientific; catalog no. 25030081). BHPrE1 cells were maintained in Dulbecco's Modified Eagle Medium/Nutrient Mixture F-12 (DMEM/F12; source; catalog no. 15-090-CV) supplemented with 5% FBS, 1% insulin-transferrin-selenium-Ethanolamine (ITS-X; Themo Fisher Scientific, Waltham, MA, USA; catalog no. 4452301), 1% penicillin-streptomycin, and 1% L-glutamine. All experiments were performed using cells between passages 10 and 25.

RNA isolation and quantitative PCR

For quantitative PCR (qPCR) analysis, total RNA was isolated from cultured prostate epithelial and prostate cancer cell lines, including BHPrE1, BPH-1, LNCaP, and C4-2 cells. RNA extraction was performed using the E.Z.N.A. Total RNA Kit (Omega Bio-Tek, Norcross, GA, USA; catalog no. R6834-02) according to the manufacturer's protocol. Reverse transcription was performed using Takara 5X PrimeScript RT Master Mix (Takara Bio, Shiga, Japan; catalog no. RR036A). qPCR was performed on a StepOnePlus Real-Time PCR System (Applied Biosystems, Foster City, CA, USA) using gene-specific primers and Bullseye Real-Time qPCR Master Mix (MidSci, Valley Park, MO, USA; catalog no. ASQPCR1). Each 10-μL reaction contained 5 μL of master mix, 0.5 μL each of 10 μM forward and reverse primers, 1 μL of template cDNA, and 3 μL of sterile ddH_2O. The cycling conditions were 95°C for 10 min, followed by 40 cycles of 95°C for 15 s and 60°C for 60 s. Relative C3 expression was calculated using the $2^{-\Delta\Delta Ct}$ method with GAPDH as the internal control. The C3 primers were designed using NCBI Primer-BLAST. The glyceraldehyde-3-phosphate dehydrogenase (GAPDH) primers were selected based on a previous report [22]. All primers were synthesized commercially (Integrated DNA Technologies, Coralville, IA, USA). The primer sequences were as follows: C3 forward, 5'-TGGCGAACAGAGGATTTCCC-3'; C3 reverse, 5'-TCTGGTAGGGAGAGGTCACG-3'; GAPDH forward, 5'-CTCCTCACAGTTGCCATGTA-3'; and GAPDH reverse, 5'-GTTGAGCACAGGG-TACTTTATTG-3'.

Western blot analysis

For Western blot analysis, protein lysates were prepared from cultured BHPrE1, BPH-1, LNCaP, and C4-2 cells. Cells were lysed in radioimmunoprecipitation assay (RIPA) prepared in the laboratory, containing 150 mM sodium chloride, 50 mM Tris-HCl (pH 8.0), 1% Nonidet P-40, 0.5% sodium deoxycholate, and 0.1% sodium dodecyl sulfate (SDS). The buffer was supplemented with 1× Pierce Protease Inhibitor Mini Tablets (Thermo Fisher Scientific, Waltham, MA, USA; catalog no. A32965) and 1 mM phenylmethylsulfonyl fluoride (PMSF; Thermo Fisher Scientific, Waltham, MA, USA; catalog no. 36978) immediately before use. Total protein was quantified using a bicinchoninic acid (BCA) protein assay. Protein extracts were boiled in SDS sample buffer and separated by SDS-polyacrylamide gel electrophoresis (SDS-PAGE). Proteins were then transferred to polyvinylidene difluoride (PVDF) membranes (Bio-Rad Laboratories, Hercules, CA, USA; catalog no. 1620177), blocked for 1 h in 5% non-fat milk, and incubated with primary antibodies at 4°C. The following primary antibodies were used: anti-C3 rabbit antibody (Abcam, Cambridge, UK; catalog no. ab200999; 1:2000) for 48 h and mouse anti-α-tubulin antibody (Santa Cruz Biotechnology, Dallas, TX, USA; catalog no. sc-8035; 1:2000) overnight. Membranes were washed in Tris-buffered saline with Tween 20 (TBST) and incubated with horseradish peroxidase (HRP)-conjugated secondary antibodies: Immun-Star Goat Anti-Rabbit (GAR)-HRP Conjugate (Bio-Rad Laboratories, Hercules, CA, USA; catalog no. 1705046; dilution 1:5000) and Immun-Star Goat Anti-Mouse (GAM)-GRP Conjugate (Bio-Rad Laboratories; catalog no. 1705047; dilution 1:5000). After additional washes in TBST, protein signals were detected using a ChemiDoc Imaging System (BioRad Laboratories, Hercules, CA, USA).

Statistical analysis

All statistical analyses were performed using R version 4.4.1 unless otherwise specified. For transcriptomic and methylation analyses, group comparisons were performed using nonparametric tests because variables derived from public datasets exhibited distributional heterogeneity and potential outliers. For comparisons between two groups, gene expression or methylation levels were evaluated using the Wilcoxon rank-sum test. For comparisons among three groups, the Kruskal-Wallis test was used, followed by pairwise Wilcoxon rank-sum tests when appropriate. *P* values from multiple comparisons were adjusted using the Benjamini-Hochberg method to control the false discovery rate (FDR).

Correlations between gene expression and promoter methylation or immune scores were assessed using Spearman's rank correlation. Univariable and multivariable linear regression analyses were performed to assess independent associations. Multivariable models included promoter methylation, immune score, and tumor status as covariates. Tumor status was treated as a categorical variable with normal tissue as the reference group.

An immune infiltration score was calculated using single-sample Gene Set Enrichment Analysis (ssGSEA) [23] implemented in the Gene Set Variation Analysis (GSVA) package [24]. The score was derived from selected Hallmark immune-related gene sets from the Molecular Signatures Database (MSigDB) [25]. To avoid circularity, the gene of interest was excluded from the complement gene set when calculating immune scores. GSEA was performed using the clusterProfiler package [26] based on genes ranked by Spearman correlation coefficients with C3 expression. Hallmark gene sets from MsigDB were used for enrichment analysis. For transcriptomic and methylation analyses, group comparisons were performed using non-parametric tests because public dataset-derived variables showed distributional heterogeneity and potential outliers. In box plots, boxes indicate the interquartile range, horizontal lines indicate the median, and whiskers indicate 1.5 times the interquartile range. A two-sided *P*-value < 0.05 or an FDR < 0.05 was considered statistically significant.

For qPCR analysis, statistical comparisons were performed using ΔCt values in GraphPad Prism 10 by one-way analysis of variance (ANOVA) followed by Dunnett's multiple comparisons test, whereas relative expression values calculated by the $2^{-\Delta\Delta Ct}$ method are shown for visualization.

Results

Altered expression patterns of complement components in prostate cancer

To obtain an overview of complement components in prostate cancer, we first evaluated log2-transformed expression levels of major complement factors, from C1 through C9, in the TCGA-PRAD dataset. As shown in **Figure 1**, multiple complement components showed statistically significant differences in expression between adjacent normal and tumor tissues. Among them, C3, C6, and C7 were significantly decreased in tumor tissues, whereas C2, C4A, C8, and C9 were significantly increased in tumors (all $P < 0.05$). Expression levels of C1 and C5 did not differ significantly between groups. After Benjamini-Hochberg correction, C2, C3, C4A, C6, C7, C8, and C9 remained significantly different between tumor and adjacent normal tissues (adjusted $P < 0.05$), indicating that complement-related changes in prostate cancer differed among individual components.

Complement component expression across clinical stages in an independent cohort

To examine whether the above findings using TCGA-PRAD were also observed in another cohort, we analyzed GSE21032, which includes 29 adjacent normal prostatic tissues, 131 primary tumors, and 19 metastatic prostate cancer samples. Five complement components (C1, C2, C3, C4A, and C7) showed significant differences among groups (Kruskal-Wallis test; adjusted $P < 0.01$ for all genes; **Figure 2**). For C2 and C4, expression levels were significantly higher in primary tumors than in adjacent normal tissues and significantly lower in metastatic lesions than in primary tumors (pairwise Wilcoxon test, adjusted $P < 0.01$). In contrast, C1, C3, and C7 did not differ significantly between adjacent normal tissues and primary tumors but were significantly lower in metastatic lesions than in primary tumors (pairwise Wilcoxon test, adjusted $P < 0.01$). Notably, all

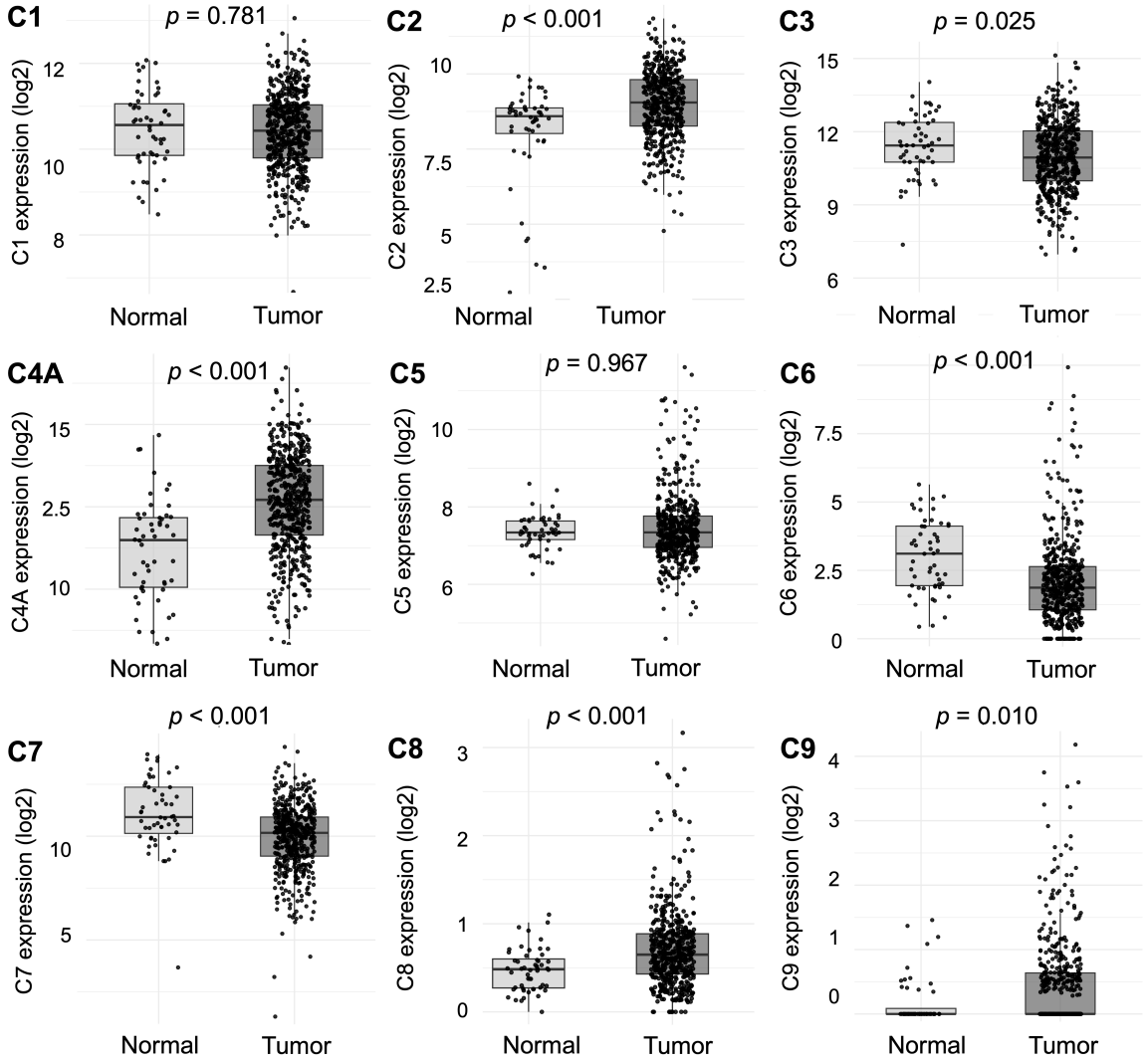


Figure 1. Differential expression of complement components in prostate cancer (TCGA-PRAD). Box-and-jitter plots showing log2-transformed expression levels of complement components (C1-C9) in tumor (n = 492) and adjacent normal prostate tissues (n = 52) from the TCGA-PRAD. For C1 and C8, mean expression values of their respective subcomponents were used. Each dot represents an individual sample. Boxes indicate the interquartile range, horizontal lines indicate the median, and whiskers indicate 1.5 times the interquartile range. Statistical significance between groups was assessed using the Wilcoxon rank-sum test. Unadjusted *p*-values are shown; adjusted *p*-values were calculated using the Benjamini-Hochberg method. TCGA-PRAD, The Cancer Genome Atlas prostate adenocarcinoma.

complement components that showed significant group differences (C1, C2, C3, C4, and C7) exhibited reduced expression in metastatic lesions compared with primary tumors, suggesting a consistent downward shift at the metastatic stage.

Promoter DNA methylation and its association with C3 expression

Given the consistent reduction in C3 and C7 across independent datasets, we next examined their promoter methylation status. GSTP1 was included as a reference gene for tumor-associated epigenetic silencing. Consistent with its established role, GSTP1 showed a strong negative correlation between expression and promoter methylation ($\rho = -0.45$, $P < 0.001$). Similarly, C3 demonstrated a significant negative correlation ($\rho = -0.28$, $P < 0.001$). In contrast, C7 showed no significant correlation between promoter methylation and gene expression ($\rho = -0.08$, $P = 0.07$). Promoter methylation levels were significantly higher

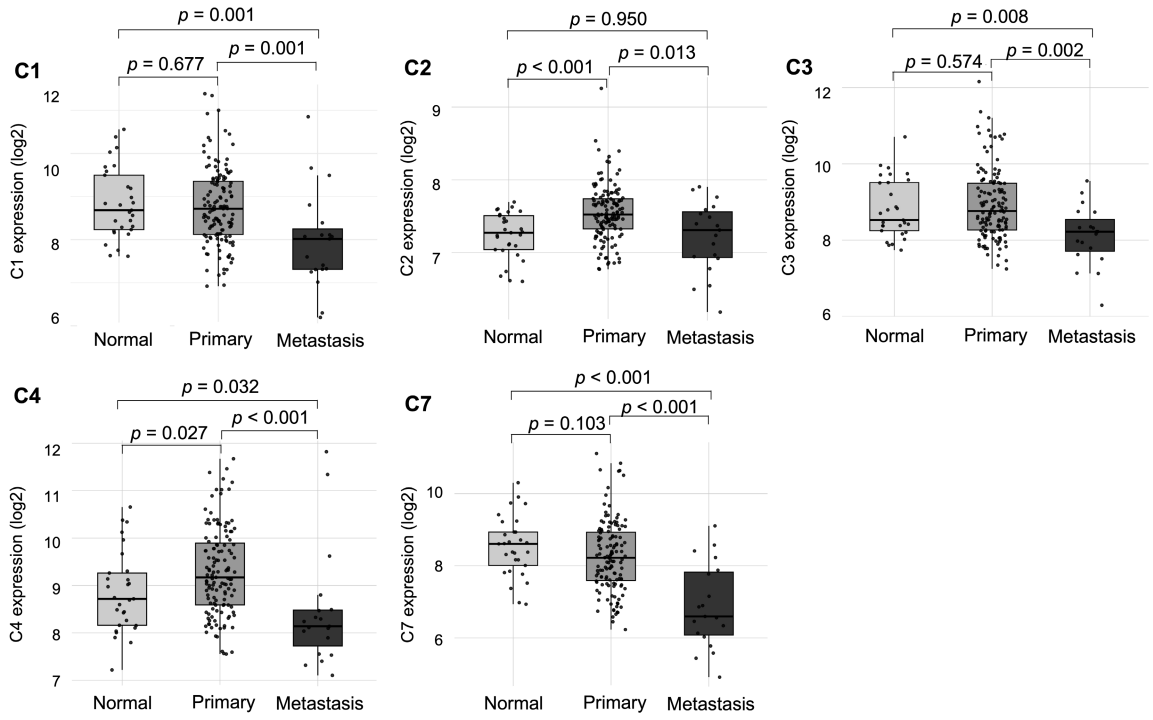


Figure 2. Complement component expression across disease states in the GSE21032 dataset. Box-and-jitter plots showing log2-transformed expression levels of complement components (C1, C2, C3, C4, and C7) in adjacent normal (n = 29), primary tumor (n = 131), and metastatic prostate tissues (n = 19) from the GSE21032 dataset. Each dot represents an individual sample. Statistical significance among groups was assessed using the Kruskal-Wallis test, followed by pairwise Wilcoxon rank-sum tests. Adjusted *p*-values (Benjamini-Hochberg method) are shown.

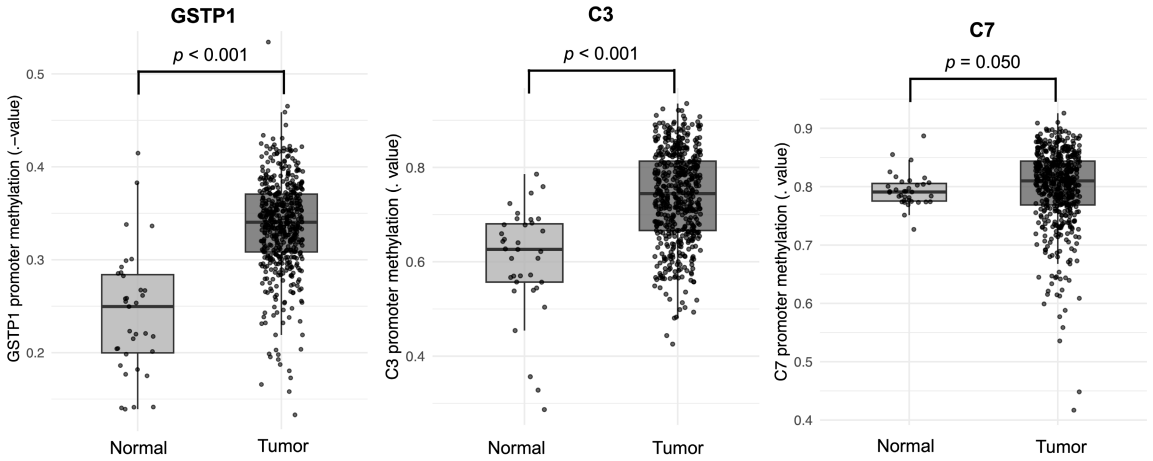


Figure 3. Promoter methylation levels of GSTP1, C3, and C7 in normal and tumor prostate tissues from TCGA-PRAD. Box-and-jitter plots showing promoter methylation levels (β values) of GSTP1, C3, and C7 in normal (n = 52) and tumor prostate tissues (n = 492) from the TCGA-PRAD dataset. Each dot represents an individual sample. Statistical significance between groups was assessed using the Wilcoxon rank-sum test. *P* values are shown above each comparison. TCGA-PRAD, The Cancer Genome Atlas prostate adenocarcinoma.

in tumor tissues for GSTP1 and C3 (P < 0.001), whereas no significant difference was observed for C7 (P = 0.050; **Figure 3**).

To evaluate the independent contributions of promoter methylation and tumor status to gene expression, multivariable linear regres-

Table 1. Multivariable linear regression analysis of promoter methylation and tumor status on gene expression in TCGA-PRAD

Gene	β (Methylation)	*p*-value (Methylation)	β (Tumor status)	*p*-value (Tumor status)
GSTP1	-9.841	< 0.001	-0.953	< 0.001
C3	-3.689	< 0.001	0.013	0.961
C7	-0.688	0.517	-0.869	0.002

Multivariable linear regression models were used to evaluate the independent contributions of promoter methylation level and tumor status to gene expression. Regression coefficients (β) and corresponding *p*-values are shown. Adjacent normal prostate tissue was used as the reference category for tumor status. GSTP1 was included as a reference gene for tumor-associated epigenetic silencing. TCGA-PRAD, The Cancer Genome Atlas prostate adenocarcinoma; GSTP1, glutathione S-transferase pi 1.

Table 2. Multivariable linear regression analysis of factors associated with C3 expression in TCGA-PRAD

Variable	β (Estimate)	Standard Error	t value	*p*-value
Promoter methylation	-1.271	0.412	-3.088	0.002
Immune score (excluding C3)	1.125	0.041	27.283	< 0.001
Tumor status	0.225	0.170	1.322	0.187

Model adjusted R^2 = 0.609. The model included promoter methylation (β value), immune score derived from single-sample Gene Set Enrichment Analysis (ssGSEA) excluding C3, and tumor status (Normal vs Tumor). Tumor status was coded with adjacent normal prostate tissue as the reference category. β coefficients represent the estimated change in C3 expression per unit increase of each variable. Standard errors, t values, and corresponding *p* values are shown. TCGA-PRAD, The Cancer Genome Atlas prostate adenocarcinoma.

sion analyses were performed (**Table 1**). After adjustment for both variables, promoter methylation remained significantly associated with C3 expression (β = -3.689, P < 0.001), whereas tumor status was not independently associated (P = 0.961). In contrast, C7 expression was independently associated with tumor status (β = -0.869, P = 0.002) but not with promoter methylation (P = 0.517). GSTP1 expression was independently associated with both promoter methylation and tumor status (both P < 0.001).

Independent association of promoter methylation and immune infiltration with C3 expression

Because complement components may reflect immune cell infiltration within the TME, we next examined whether the association between promoter methylation and C3 expression could be explained by differences in immune composition. An ssGSEA-derived immune score was calculated after excluding C3 from the complement gene set to avoid circularity. The immune score was strongly associated with C3 expression (β = 0.79, P < 0.001).

We then performed multivariable linear regression including promoter methylation, immune score, and tumor status (**Table 2**). Both promoter methylation (β = -1.27, P = 0.002) and immune score (β = 1.12, P < 0.001) remained independently associated with expression, whereas tumor status was not significant. Similar results were observed when the analysis was restricted to tumor samples alone, with promoter methylation and immune score remaining independently associated with C3 expression (Supplementary Table 1).

Functional enrichment analysis of pathways negatively associated with C3 expression

To explore the biological pathways associated with reduced C3 expression, we performed Gene Set Enrichment Analysis (GSEA) using the Hallmark gene sets ranked by Spearman correlation with C3 expression in TCGA-PRAD. Instead of dividing samples into C3 high and low groups, genes were ranked according to their correlation with C3 expression.

Six Hallmark pathways were significantly enriched among genes negatively correlated with C3 expression (FDR < 0.05; Supplementary Table 2). The most prominent pathway was HALLMARK_MYC_TARGETS_V2 (normalized enrichment score (NES) = -2.60, FDR < 0.001), followed by HALLMARK_ANDROGEN_RESPONSE (NES = -2.19, FDR < 0.001). Additional significantly enriched pathways included HALLMARK_UNFORLDED_PROTEIN_RESPONSE, HALLMARK_PROTEIN_SECRETION, HALLMARK_PEROXISOME, and HALLMARK_CHOLESTEROL_HOMEOSTASIS (**Figure 4** and Supplementary Tables 2, 3). These results suggest that reduced C3 expression is associated with

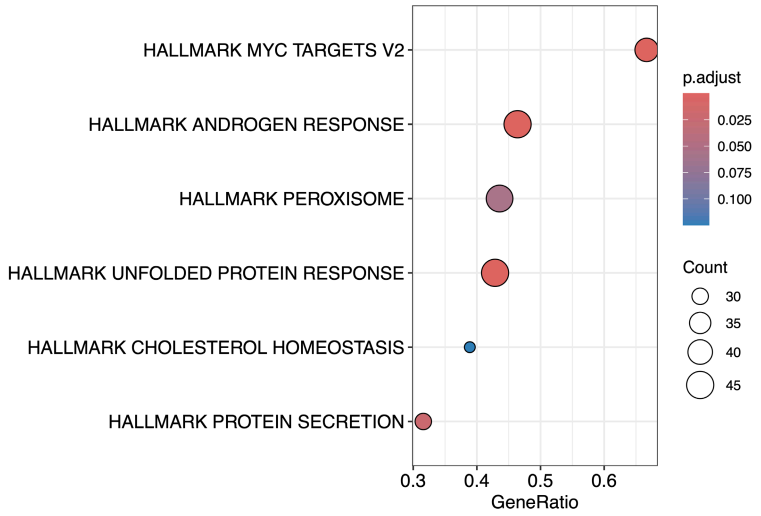


Figure 4. Hallmark pathways negatively associated with C3 expression in TCGA-PRAD. Dot plot showing Hallmark gene sets significantly enriched among genes negatively correlated with C3 expression in TCGA-PRAD. Gene sets were ranked by Spearman correlation with C3 expression and analyzed by Gene Set Enrichment Analysis (GSEA). Only pathways with negative normalized enrichment scores are displayed. The x-axis represents the GeneRatio, defined as the proportion of genes within each pathway contributing to the enrichment signal. Dot size shows the number of contributing genes, and color represents the false discovery rate (FDR)-adjusted *p* value (p.adjust). TCGA-PRAD, The Cancer Genome Atlas prostate adenocarcinoma.

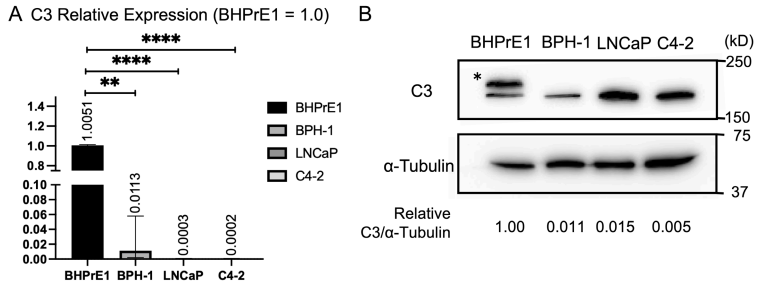


Figure 5. C3 Expression in Benign and Malignant Prostate Cell Lines. C3 expression in benign and malignant prostate cell lines. A. Relative C3 messenger RNA (mRNA) expression in benign prostate epithelial cell lines (BHPrE1 and BPH-1) and malignant prostate cell lines (LNCaP and C4-2). Expression levels were normalized to BHPrE1 and are shown relative to BHPrE1 = 1.0. Data are shown as mean ± standard deviation (SD) from three independent experiments. The y-axis is shown with a break to improve visualization of low-expression groups. Statistical analysis was performed using one-way analysis of variance (ANOVA) with multiple comparisons. **P < 0.01, ****P < 0.0001. B. Representative Western blot showing C3 protein expression in the indicated cell lines, with α-tubulin as a loading control (50 kDa). The asterisk indicates the upper band corresponding to putative full-length C3 (187 kDa). Densitometric quantification was performed for the upper C3 band corresponding to putative full-length C3. C3 band intensities were background-subtracted, normalized to α-tubulin, and expressed relative to BHPrE1.

MYC-driven transcriptional programs, androgen signaling, and metabolic pathways in prostate cancer.

Reduced C3 expression in prostate cancer cell lines

To further examine C3 expression at the cellular level, we evaluated C3 expression in benign and malignant prostate cell lines. C3 mRNA expression was significantly reduced in BPH-1, LNCaP, and C4-2 cells compared with BHPrE1 cells (adjusted P = 0.0029, P < 0.0001, P < 0.0001, respectively; **Figure 5A**). Consistent with the mRNA findings, western blot analysis also showed reduced C3 protein expression in LNCaP and C4-2 cells relative to BHPrE1 cells (**Figure 5B**). Interestingly, the immortalized benign prostatic epithelial cell line BPH-1, which is often used as a model of non-malignant prostatic epithelial cells or precursor of prostate cancer [27], also showed reduced C3 expression compared with BHPrE1, an immortalized prostatic epithelial cells capable of regenerating benign secretory ductal-acinar architecture in vivo [28], although not to the same extent as the prostate cancer cell lines (**Figure 5A**). These findings suggest that C3 downregulation is prominent in prostate cancer cells, while partial reduction may also be present in some non-malignant prostatic epithelial cells.

Discussion

In this study, we found that multiple complement factors were differentially expressed among normal, primary tumor, and metastatic samples, suggesting that complement dysregulation is associated with clinical states of prostate cancer. Among these factors, C3 showed the most consistent decrease across datasets and was associated with promoter methylation inde-

pendently of immune-related variation. These findings suggest that C3 downregulation in prostate cancer may reflect both immune-related variation in the tumor microenvironment and epigenetic regulation associated with promoter methylation.

Complement dysregulation across disease states in prostate cancer

Across two independent datasets, we observed consistent alterations in multiple complement components in prostate cancer. Classical pathway components, including C2 and C4, were upregulated in primary tumors compared with normal tissues in both TCGA-PRAD and GSE-21032, but their expression declined in metastatic lesions. Similarly, C3 and C7 were significantly reduced in tumor tissues relative to normal prostate in TCGA and showed further downregulation in metastatic samples in GSE21032. Taken together, these findings suggest that metastatic prostate cancer is characterized by reduced expression of several complement components.

In our analysis of the publicly available datasets, not all complement components showed consistent transcriptional alterations across disease states. In particular, C5 expression did not change significantly at the mRNA level across the datasets analyzed in this study. Nevertheless, previous studies have demonstrated that C5a signaling enhances prostate cancer cell proliferation, invasion, and programmed death-ligand 1 (PD-L1) expression [9, 29]. This suggests that complement activity may be regulated at levels beyond transcription, including ligand cleavage and receptor-mediated signaling.

Consistent with the transcriptomic findings, C3 expression was also reduced in prostate cancer cell lines at both the mRNA and protein levels. The detection of C3 in benign prostatic epithelial cells supports that C3 expression in bulk tissue datasets may reflect not only non-epithelial components such as infiltrating immune cells, but also prostatic epithelial cells themselves. Partial reduction in BPH-1 cells further suggests that C3 downregulation may not be entirely restricted to malignant cells.

Distinct regulatory patterns of C3 and C7

DNA promoter methylation is a well-established mechanism of transcriptional silencing in cancer [30]. Complement components can be produced by both tumor and infiltrating immune cells [31], raising the possibility that differences in immune composition may influence bulk tumor expression profiles. After adjustment for immune infiltration, promoter methylation remained independently associated with C3 expression, suggesting that epigenetic regulation contributes to C3 downregulation in prostate cancer. To our knowledge, this relationship has not been systematically examined in prostate cancer.

In contrast, C7 showed no significant association with promoter methylation in multivariable analyses. Instead, C7 expression was independently associated with both immune score and tumor status. Previous studies have described C7 as an immune-related biomarker in prostate cancer [32], and androgen-regulated stromal expression of C7 has been reported to suppress prostate cancer growth [33]. Together, these findings suggest that C7 expression may reflect microenvironmental variation rather than an epigenetic silencing within tumor cells.

Low C3 expression is associated with MYC-driven and androgen-responsive transcriptional programs

GSEA analysis revealed that reduced C3 expression was significantly associated with MYC target gene sets and androgen receptor (AR) pathways. MYC and AR are major drivers of prostate cancer progression and tumor proliferation [3, 18]. In addition, the unfolded protein response (UPR) pathway was enriched in tumors with low C3 expression. UPR reflects endoplasmic reticulum (ER) stress and increased protein synthesis demand, which are commonly observed in rapidly proliferating tumors [34, 35]. These findings suggest that reduced C3 expression may be associated with transcriptional programs characteristic of proliferative and aggressive tumor states. Although the present data do not establish causality, reduced C3 expression may mark a transcriptional state associated with tumor aggressiveness in prostate cancer.

Limitations

Several limitations of this study should be acknowledged. First, this study was based on publicly available transcriptomic and methyla-

tion datasets derived from bulk tumor samples. Although we adjusted for immune infiltration to account for differences in cellular composition, bulk transcriptomic data cannot fully distinguish tumor-intrinsic expression from signals generated from other cell types. Second, this study was an observational analysis. The relationships between C3 expression, promoter methylation, and proliferative transcriptional programs should be interpreted as associations rather than evidence of causality. Functional studies are needed to determine whether promoter methylation directly contributes to C3 downregulation. Finally, mRNA expression does not necessarily reflect complement activity in tumor tissue. C3 activation also depends on protein cleavage, receptor signaling, and local conditions within the tumor microenvironment.

Conclusion

C3 is downregulated in prostate cancer and is associated with promoter methylation and immune context. These findings suggest that C3 dysregulation reflects both tumor-intrinsic epigenetic regulation and the tumor microenvironment, supporting further investigation of its role in prostate cancer progression.

Acknowledgements

The work was supported by a grant from the National Institutes of Health (R01 DK134580 to NY & ZW).

Disclosure of conflict of interest

None.

Address correspondence to: Naoki Yoshimura, Department of Urology, University of Pittsburgh School of Medicine, Suite 700 Kaufmann Medical Building, 3471 Fifth Avenue, Pittsburgh, PA 15213, USA. E-mail: nyos@pitt.edu; Zhou Wang, Department of Urology, Shadyside Medical Center, 5200 Center Avenue, Suite G40, Pittsburgh, PA 15232, USA. E-mail: wangz2@upmc.edu

References

[1] Sung H, Ferlay J, Siegel RL, Laversanne M, Soerjomataram I, Jemal A and Bray F. Global cancer statistics 2020: GLOBOCAN estimates of incidence and mortality worldwide for 36 cancers in 185 countries. CA Cancer J Clin 2021; 71: 209-249.

[2] Kania E, Janica M, Nesterowicz M, Modzelewski W, Cybulski M and Janica J. Advances and challenges in prostate cancer diagnosis: a comprehensive review. Cancers (Basel) 2025; 17: 2137.

[3] Watson PA, Arora VK and Sawyers CL. Emerging mechanisms of resistance to androgen receptor inhibitors in prostate cancer. Nat Rev Cancer 2015; 15: 701-711.

[4] Stultz J and Fong L. How to turn up the heat on the cold immune microenvironment of metastatic prostate cancer. Prostate Cancer Prostatic Dis 2021; 24: 697-717.

[5] Kukkonen K, Taavitsainen S, Huhtala L, Uusi-Makela J, Granberg KJ, Nykter M and Urbanucci A. Chromatin and epigenetic dysregulation of prostate cancer development, progression, and therapeutic response. Cancers (Basel) 2021; 13: 3325.

[6] Zhang R, Liu Q, Li T, Liao Q and Zhao Y. Role of the complement system in the tumor microenvironment. Cancer Cell Int 2019; 19: 300.

[7] Artero MR, Minery A, Nedelcev L, Radanova M and Roumenina LT. Complement and the hallmarks of cancer. Semin Immunol 2025; 78: 101950.

[8] Ain D, Shaikh T, Manimala S and Ghebrehiwet B. The role of complement in the tumor microenvironment. Fac Rev 2021; 10: 80.

[9] Stallone G, Netti GS, Cormio L, Castellano G, Infante B, Pontrelli P, Divella C, Selvaggio O, Spadaccino F, Ranieri E, Sanguedolce F, Pennella A, Gesualdo L, Carrieri G and Grandaliano G. Modulation of complement activation by pentraxin-3 in prostate cancer. Sci Rep 2020; 10: 18400.

[10] Roumenina LT, Daugan MV, Petitprez F, Sautès-Fridman C and Fridman WH. Context-dependent roles of complement in cancer. Nat Rev Cancer 2019; 19: 698-715.

[11] Park JY. Promoter hypermethylation in prostate cancer. Cancer Control 2010; 17: 245-255.

[12] Henrique R and Jerónimo C. Molecular detection of prostate cancer: a role for GSTP1 hypermethylation. Eur Urol 2004; 46: 660-669; discussion 669.

[13] Jerónimo C, Usadel H, Henrique R, Oliveira J, Lopes C, Nelson WG and Sidransky D. Quantitation of GSTP1 methylation in non-neoplastic prostatic tissue and organ-confined prostate adenocarcinoma. J Natl Cancer Inst 2001; 93: 1747-1752.

[14] Cancer Genome Atlas Research Network. The molecular taxonomy of primary prostate cancer. Cell 2015; 163: 1011-1025.

[15] Goldman MJ, Craft B, Hastie M, Repečka K, McDade F, Kamath A, Banerjee A, Luo Y, Rogers D, Brooks AN, Zhu J and Haussler D. Visual-

izing and interpreting cancer genomics data via the Xena platform. Nat Biotechnol 2020; 38: 675-678.
[16] Li B and Dewey CN. RSEM: accurate transcript quantification from RNA-Seq data with or without a reference genome. BMC Bioinformatics 2011; 12: 323.
[17] Bibikova M, Barnes B, Tsan C, Ho V, Klotzle B, Le JM, Delano D, Zhang L, Schroth GP, Gunderson KL, Fan JB and Shen R. High density DNA methylation array with single CpG site resolution. Genomics 2011; 98: 288-295.
[18] Taylor BS, Schultz N, Hieronymus H, Gopalan A, Xiao Y, Carver BS, Arora VK, Kaushik P, Cerami E, Reva B, Antipin Y, Mitsiades N, Landers T, Dolgalev I, Major JE, Wilson M, Socci ND, Lash AE, Heguy A, Eastham JA, Scher HI, Reuter VE, Scardino PT, Sander C, Sawyers CL and Gerald WL. Integrative genomic profiling of human prostate cancer. Cancer Cell 2010; 18: 11-22.
[19] Irizarry RA, Hobbs B, Collin F, Beazer-Barclay YD, Antonellis KJ, Scherf U and Speed TP. Exploration, normalization, and summaries of high density oligonucleotide array probe level data. Biostatistics 2003; 4: 249-264.
[20] Cole RN, Chen W, Pascal LE, Nelson JB, Wipf P and Wang Z. (+)-JJ-74-138 is a novel noncompetitive androgen receptor antagonist. Mol Cancer Ther 2022; 21: 483-492.
[21] Li F, Pascal LE, Wang K, Zhou Y, Balasubramani GK, O'Malley KJ, Dhir R, He K, Stolz D, DeFranco DB, Yoshimura N, Nelson JB, Chong T, Guo P, He D and Wang Z. Transforming growth factor beta 1 impairs benign prostatic luminal epithelial cell monolayer barrier function. Am J Clin Exp Urol 2020; 8: 9-17.
[22] Lv S, Wu Z, Luo M, Zhang Y, Zhang J, Pascal LE, Wang Z and Wei Q. Integrated analysis reveals FOXA1 and Ku70/Ku80 as targets of ivermectin in prostate cancer. Cell Death Dis 2022; 13: 754.
[23] Barbie DA, Tamayo P, Boehm JS, Kim SY, Moody SE, Dunn IF, Schinzel AC, Sandy P, Meylan E, Scholl C, Fröhling S, Chan EM, Sos ML, Michel K, Mermel C, Silver SJ, Weir BA, Reiling JH, Sheng Q, Gupta PB, Wadlow RC, Le H, Hoersch S, Wittner BS, Ramaswamy S, Livingston DM, Sabatini DM, Meyerson M, Thomas RK, Lander ES, Mesirov JP, Root DE, Gilliland DG, Jacks T and Hahn WC. Systematic RNA interference reveals that oncogenic KRAS-driven cancers require TBK1. Nature 2009; 462: 108-112.
[24] Hänzelmann S, Castelo R and Guinney J. GSVA: gene set variation analysis for microarray and RNA-seq data. BMC Bioinformatics 2013; 14: 7.
[25] Liberzon A, Birger C, Thorvaldsdóttir H, Ghandi M, Mesirov JP and Tamayo P. The Molecular Signatures Database (MSigDB) hallmark gene set collection. Cell Syst 2015; 1: 417-425.
[26] Yu G, Wang LG, Han Y and He QY. clusterProfiler: an R package for comparing biological themes among gene clusters. OMICS 2012; 16: 284-287.
[27] Hayward SW, Wang Y, Cao M, Hom YK, Zhang B, Grossfeld GD, Sudilovsky D and Cunha GR. Malignant transformation in a nontumorigenic human prostatic epithelial cell line. Cancer Res 2001; 61: 8135-8142.
[28] Jiang M, Strand DW, Fernandez S, He Y, Yi Y, Birbach A, Qiu Q, Schmid J, Tang DG and Hayward SW. Functional remodeling of benign human prostatic tissues in vivo by spontaneously immortalized progenitor and intermediate cells. Stem Cells 2010; 28: 344-356.
[29] Imamura R, Kitagawa S, Kubo T, Irie A, Kariu T, Yoneda M, Kamba T and Imamura T. Prostate cancer C5a receptor expression and augmentation of cancer cell proliferation, invasion, and PD-L1 expression by C5a. Prostate 2021; 81: 147-156.
[30] Baylin SB. DNA methylation and gene silencing in cancer. Nat Clin Pract Oncol 2005; 2 Suppl 1: S4-11.
[31] Kolev M, Le Friec G and Kemper C. Complement--tapping into new sites and effector systems. Nat Rev Immunol 2014; 14: 811-820.
[32] Chen Z, Yan X, Du GW, Tuoheti K, Bai XJ, Wu HH, Zhang RJ, Xiao GF and Liu TZ. Complement C7 (C7), a potential tumor suppressor, is an immune-related prognostic biomarker in prostate cancer (PC). Front Oncol 2020; 10: 1532.
[33] Zhou Z, Jia D, Kwon O, Li S, Sun H, Roudier MP, Lin DW, True L, Morrissey C, Creighton CJ, Lee JK and Xin L. Androgen-regulated stromal complement component 7 (C7) suppresses prostate cancer growth. Oncogene 2023; 42: 2428-2438.
[34] Clarke HJ, Chambers JE, Liniker E and Marciniak SJ. Endoplasmic reticulum stress in malignancy. Cancer Cell 2014; 25: 563-573.
[35] Hetz C and Papa FR. The unfolded protein response and cell fate control. Mol Cell 2018; 69: 169-181.

Supplementary Table 1. Multivariable linear regression analysis of C3 expression restricted to tumor samples

Gene	Variable	β (Estimate)	Standard Errors	t value	*p*-value
C3	Promoter methylation	-0.99	0.42	-2.34	0.020
	Immune score	1.15	0.04	27.89	< 0.001

Model adjusted R^2 = 0.630. The immune score was calculated using single-sample Gene Set Enrichment Analysis (ssGSEA) after excluding the gene of interest from the complement gene. β coefficients, standard errors, t values, *p*-values, and model-adjusted R^2 are shown.

Supplementary Table 2. Hallmark gene sets negatively enriched according to Spearman correlation with C3 expression in TCGA-PRAD

Description	setSize	NES	*p* value	p.adjust
HALLMARK_MYC_TARGETS_V2	57	-2.598	9.46E-09	2.91E-08
HALLMARK_ANDROGEN_RESPONSE	97	-2.191	3.47E-08	9.32E-08
HALLMARK_UNFOLDED_PROTEIN_RESPONSE	105	-1.921	8.01E-07	1.86E-06
HALLMARK_PROTEIN_SECRETION	95	-1.361	0.0138	0.0212
HALLMARK_PEROXISOME	101	-1.203	0.0375	0.0556
HALLMARK_CHOLESTEROL_HOMEOSTASIS	72	-1.194	0.091	0.125

Supplementary Table 3. Leading-edge genes for significantly enriched Hallmark pathways

Pathway	NES	FDR	Gene
HALLMARK_MYC_TARGETS_V2	-2.612E+00	7.314E-09	PRMT3
HALLMARK_MYC_TARGETS_V2	-2.612E+00	7.314E-09	PES 1.00
HALLMARK_MYC_TARGETS_V2	-2.612E+00	7.314E-09	SUPV3L1
HALLMARK_MYC_TARGETS_V2	-2.612E+00	7.314E-09	CBX3
HALLMARK_MYC_TARGETS_V2	-2.612E+00	7.314E-09	RABEPK
HALLMARK_MYC_TARGETS_V2	-2.612E+00	7.314E-09	IMP4
HALLMARK_MYC_TARGETS_V2	-2.612E+00	7.314E-09	NOP56
HALLMARK_MYC_TARGETS_V2	-2.612E+00	7.314E-09	SORD
HALLMARK_MYC_TARGETS_V2	-2.612E+00	7.314E-09	NOLC1
HALLMARK_MYC_TARGETS_V2	-2.612E+00	7.314E-09	NOC4L
HALLMARK_MYC_TARGETS_V2	-2.612E+00	7.314E-09	CDK4
HALLMARK_MYC_TARGETS_V2	-2.612E+00	7.314E-09	UNG
HALLMARK_MYC_TARGETS_V2	-2.612E+00	7.314E-09	TBRG4
HALLMARK_MYC_TARGETS_V2	-2.612E+00	7.314E-09	LAS1L
HALLMARK_MYC_TARGETS_V2	-2.612E+00	7.314E-09	RRP12
HALLMARK_MYC_TARGETS_V2	-2.612E+00	7.314E-09	PPAN
HALLMARK_MYC_TARGETS_V2	-2.612E+00	7.314E-09	NOP2
HALLMARK_MYC_TARGETS_V2	-2.612E+00	7.314E-09	WDR74
HALLMARK_MYC_TARGETS_V2	-2.612E+00	7.314E-09	NPM1
HALLMARK_MYC_TARGETS_V2	-2.612E+00	7.314E-09	IPO4
HALLMARK_MYC_TARGETS_V2	-2.612E+00	7.314E-09	MYBBP1A
HALLMARK_MYC_TARGETS_V2	-2.612E+00	7.314E-09	RRP9
HALLMARK_MYC_TARGETS_V2	-2.612E+00	7.314E-09	SRM
HALLMARK_MYC_TARGETS_V2	-2.612E+00	7.314E-09	EXOSC5
HALLMARK_MYC_TARGETS_V2	-2.612E+00	7.314E-09	NOP16
HALLMARK_MYC_TARGETS_V2	-2.612E+00	7.314E-09	PA2G4
HALLMARK_MYC_TARGETS_V2	-2.612E+00	7.314E-09	MRTO4

HALLMARK_MYC_TARGETS_V2	-2.612E+00	7.314E-09	TFB2M
HALLMARK_MYC_TARGETS_V2	-2.612E+00	7.314E-09	AIMP2
HALLMARK_MYC_TARGETS_V2	-2.612E+00	7.314E-09	HSPD1
HALLMARK_MYC_TARGETS_V2	-2.612E+00	7.314E-09	SLC19A1
HALLMARK_MYC_TARGETS_V2	-2.612E+00	7.314E-09	SLC29A2
HALLMARK_MYC_TARGETS_V2	-2.612E+00	7.314E-09	BYSL
HALLMARK_MYC_TARGETS_V2	-2.612E+00	7.314E-09	TMEM97
HALLMARK_MYC_TARGETS_V2	-2.612E+00	7.314E-09	HSPE1
HALLMARK_MYC_TARGETS_V2	-2.612E+00	7.314E-09	FARSA
HALLMARK_MYC_TARGETS_V2	-2.612E+00	7.314E-09	GNL3
HALLMARK_MYC_TARGETS_V2	-2.612E+00	7.314E-09	MPHOSPH10
HALLMARK_ANDROGEN_RESPONSE	-2.185E+00	4.105E-08	ELK4
HALLMARK_ANDROGEN_RESPONSE	-2.185E+00	4.105E-08	ZBTB10
HALLMARK_ANDROGEN_RESPONSE	-2.185E+00	4.105E-08	PGM3
HALLMARK_ANDROGEN_RESPONSE	-2.185E+00	4.105E-08	INSIG1
HALLMARK_ANDROGEN_RESPONSE	-2.185E+00	4.105E-08	SORD
HALLMARK_ANDROGEN_RESPONSE	-2.185E+00	4.105E-08	MERTK
HALLMARK_ANDROGEN_RESPONSE	-2.185E+00	4.105E-08	ADRM1
HALLMARK_ANDROGEN_RESPONSE	-2.185E+00	4.105E-08	IDI1
HALLMARK_ANDROGEN_RESPONSE	-2.185E+00	4.105E-08	IQGAP2
HALLMARK_ANDROGEN_RESPONSE	-2.185E+00	4.105E-08	RRP12
HALLMARK_ANDROGEN_RESPONSE	-2.185E+00	4.105E-08	HERC3
HALLMARK_ANDROGEN_RESPONSE	-2.185E+00	4.105E-08	SCD
HALLMARK_ANDROGEN_RESPONSE	-2.185E+00	4.105E-08	DHCR24
HALLMARK_ANDROGEN_RESPONSE	-2.185E+00	4.105E-08	DBI
HALLMARK_ANDROGEN_RESPONSE	-2.185E+00	4.105E-08	KRT8
HALLMARK_ANDROGEN_RESPONSE	-2.185E+00	4.105E-08	HMGCR
HALLMARK_ANDROGEN_RESPONSE	-2.185E+00	4.105E-08	ELL2
HALLMARK_ANDROGEN_RESPONSE	-2.185E+00	4.105E-08	STEAP4
HALLMARK_ANDROGEN_RESPONSE	-2.185E+00	4.105E-08	PA2G4
HALLMARK_ANDROGEN_RESPONSE	-2.185E+00	4.105E-08	UBE2J1
HALLMARK_ANDROGEN_RESPONSE	-2.185E+00	4.105E-08	SRP19
HALLMARK_ANDROGEN_RESPONSE	-2.185E+00	4.105E-08	MAP7
HALLMARK_ANDROGEN_RESPONSE	-2.185E+00	4.105E-08	TMPRSS2
HALLMARK_ANDROGEN_RESPONSE	-2.185E+00	4.105E-08	TMEM50A
HALLMARK_ANDROGEN_RESPONSE	-2.185E+00	4.105E-08	PDLIM5
HALLMARK_ANDROGEN_RESPONSE	-2.185E+00	4.105E-08	ELOVL5
HALLMARK_ANDROGEN_RESPONSE	-2.185E+00	4.105E-08	CENPN
HALLMARK_ANDROGEN_RESPONSE	-2.185E+00	4.105E-08	ALDH1A3
HALLMARK_ANDROGEN_RESPONSE	-2.185E+00	4.105E-08	ABCC4
HALLMARK_ANDROGEN_RESPONSE	-2.185E+00	4.105E-08	ACSL3
HALLMARK_ANDROGEN_RESPONSE	-2.185E+00	4.105E-08	TARP
HALLMARK_ANDROGEN_RESPONSE	-2.185E+00	4.105E-08	AKT1
HALLMARK_ANDROGEN_RESPONSE	-2.185E+00	4.105E-08	STK39
HALLMARK_ANDROGEN_RESPONSE	-2.185E+00	4.105E-08	HOMER2
HALLMARK_ANDROGEN_RESPONSE	-2.185E+00	4.105E-08	SMS
HALLMARK_ANDROGEN_RESPONSE	-2.185E+00	4.105E-08	RAB4A
HALLMARK_ANDROGEN_RESPONSE	-2.185E+00	4.105E-08	NKX3-1
HALLMARK_ANDROGEN_RESPONSE	-2.185E+00	4.105E-08	TPD52

HALLMARK_ANDROGEN_RESPONSE	-2.185E+00	4.105E-08	UAP1
HALLMARK_ANDROGEN_RESPONSE	-2.185E+00	4.105E-08	BMPR1B
HALLMARK_ANDROGEN_RESPONSE	-2.185E+00	4.105E-08	CAMKK2
HALLMARK_ANDROGEN_RESPONSE	-2.185E+00	4.105E-08	PMEPA1
HALLMARK_ANDROGEN_RESPONSE	-2.185E+00	4.105E-08	SPDEF
HALLMARK_ANDROGEN_RESPONSE	-2.185E+00	4.105E-08	KLK2
HALLMARK_ANDROGEN_RESPONSE	-2.185E+00	4.105E-08	KLK3
HALLMARK_UNFOLDED_PROTEIN_RESPONSE	-1.870E+00	1.500E-06	ARFGAP1
HALLMARK_UNFOLDED_PROTEIN_RESPONSE	-1.870E+00	1.500E-06	NOP56
HALLMARK_UNFOLDED_PROTEIN_RESPONSE	-1.870E+00	1.500E-06	SLC30A5
HALLMARK_UNFOLDED_PROTEIN_RESPONSE	-1.870E+00	1.500E-06	POP4
HALLMARK_UNFOLDED_PROTEIN_RESPONSE	-1.870E+00	1.500E-06	NOLC1
HALLMARK_UNFOLDED_PROTEIN_RESPONSE	-1.870E+00	1.500E-06	SLC1A4
HALLMARK_UNFOLDED_PROTEIN_RESPONSE	-1.870E+00	1.500E-06	RPS14
HALLMARK_UNFOLDED_PROTEIN_RESPONSE	-1.870E+00	1.500E-06	SEC11A
HALLMARK_UNFOLDED_PROTEIN_RESPONSE	-1.870E+00	1.500E-06	EIF4G1
HALLMARK_UNFOLDED_PROTEIN_RESPONSE	-1.870E+00	1.500E-06	SSR1
HALLMARK_UNFOLDED_PROTEIN_RESPONSE	-1.870E+00	1.500E-06	CNOT6
HALLMARK_UNFOLDED_PROTEIN_RESPONSE	-1.870E+00	1.500E-06	ASNS
HALLMARK_UNFOLDED_PROTEIN_RESPONSE	-1.870E+00	1.500E-06	PAIP1
HALLMARK_UNFOLDED_PROTEIN_RESPONSE	-1.870E+00	1.500E-06	HSPA5
HALLMARK_UNFOLDED_PROTEIN_RESPONSE	-1.870E+00	1.500E-06	PDIA6
HALLMARK_UNFOLDED_PROTEIN_RESPONSE	-1.870E+00	1.500E-06	SRPRB
HALLMARK_UNFOLDED_PROTEIN_RESPONSE	-1.870E+00	1.500E-06	XPOT
HALLMARK_UNFOLDED_PROTEIN_RESPONSE	-1.870E+00	1.500E-06	NFYA
HALLMARK_UNFOLDED_PROTEIN_RESPONSE	-1.870E+00	1.500E-06	ALDH18A1
HALLMARK_UNFOLDED_PROTEIN_RESPONSE	-1.870E+00	1.500E-06	NPM1
HALLMARK_UNFOLDED_PROTEIN_RESPONSE	-1.870E+00	1.500E-06	HYOU1
HALLMARK_UNFOLDED_PROTEIN_RESPONSE	-1.870E+00	1.500E-06	BANF1
HALLMARK_UNFOLDED_PROTEIN_RESPONSE	-1.870E+00	1.500E-06	EXOSC9
HALLMARK_UNFOLDED_PROTEIN_RESPONSE	-1.870E+00	1.500E-06	TUBB2A
HALLMARK_UNFOLDED_PROTEIN_RESPONSE	-1.870E+00	1.500E-06	RRP9
HALLMARK_UNFOLDED_PROTEIN_RESPONSE	-1.870E+00	1.500E-06	HSP90B1
HALLMARK_UNFOLDED_PROTEIN_RESPONSE	-1.870E+00	1.500E-06	ATF4
HALLMARK_UNFOLDED_PROTEIN_RESPONSE	-1.870E+00	1.500E-06	EXOSC5
HALLMARK_UNFOLDED_PROTEIN_RESPONSE	-1.870E+00	1.500E-06	LSM 4.00
HALLMARK_UNFOLDED_PROTEIN_RESPONSE	-1.870E+00	1.500E-06	PREB
HALLMARK_UNFOLDED_PROTEIN_RESPONSE	-1.870E+00	1.500E-06	EIF4E
HALLMARK_UNFOLDED_PROTEIN_RESPONSE	-1.870E+00	1.500E-06	IMP3
HALLMARK_UNFOLDED_PROTEIN_RESPONSE	-1.870E+00	1.500E-06	EIF4A1
HALLMARK_UNFOLDED_PROTEIN_RESPONSE	-1.870E+00	1.500E-06	EXOSC4
HALLMARK_UNFOLDED_PROTEIN_RESPONSE	-1.870E+00	1.500E-06	NHP2
HALLMARK_UNFOLDED_PROTEIN_RESPONSE	-1.870E+00	1.500E-06	EEF2
HALLMARK_UNFOLDED_PROTEIN_RESPONSE	-1.870E+00	1.500E-06	SPCS1
HALLMARK_UNFOLDED_PROTEIN_RESPONSE	-1.870E+00	1.500E-06	DNAJA4
HALLMARK_UNFOLDED_PROTEIN_RESPONSE	-1.870E+00	1.500E-06	PDIA5
HALLMARK_UNFOLDED_PROTEIN_RESPONSE	-1.870E+00	1.500E-06	HSPA9
HALLMARK_UNFOLDED_PROTEIN_RESPONSE	-1.870E+00	1.500E-06	DKC1
HALLMARK_UNFOLDED_PROTEIN_RESPONSE	-1.870E+00	1.500E-06	YIF1A

HALLMARK_UNFOLDED_PROTEIN_RESPONSE	-1.870E+00	1.500E-06	SERP1
HALLMARK_UNFOLDED_PROTEIN_RESPONSE	-1.870E+00	1.500E-06	CALR
HALLMARK_UNFOLDED_PROTEIN_RESPONSE	-1.870E+00	1.500E-06	PSAT1
HALLMARK_PROTEIN_SECRETION	-1.345E+00	2.909E-02	RAB5A
HALLMARK_PROTEIN_SECRETION	-1.345E+00	2.909E-02	ATP6V1H
HALLMARK_PROTEIN_SECRETION	-1.345E+00	2.909E-02	ARCN1
HALLMARK_PROTEIN_SECRETION	-1.345E+00	2.909E-02	OCRL
HALLMARK_PROTEIN_SECRETION	-1.345E+00	2.909E-02	ERGIC3
HALLMARK_PROTEIN_SECRETION	-1.345E+00	2.909E-02	SEC22B
HALLMARK_PROTEIN_SECRETION	-1.345E+00	2.909E-02	YKT6
HALLMARK_PROTEIN_SECRETION	-1.345E+00	2.909E-02	SOD1
HALLMARK_PROTEIN_SECRETION	-1.345E+00	2.909E-02	COPB2
HALLMARK_PROTEIN_SECRETION	-1.345E+00	2.909E-02	CLTA
HALLMARK_PROTEIN_SECRETION	-1.345E+00	2.909E-02	SCAMP1
HALLMARK_PROTEIN_SECRETION	-1.345E+00	2.909E-02	TMED10
HALLMARK_PROTEIN_SECRETION	-1.345E+00	2.909E-02	DNM1L
HALLMARK_PROTEIN_SECRETION	-1.345E+00	2.909E-02	SNAP23
HALLMARK_PROTEIN_SECRETION	-1.345E+00	2.909E-02	AP2S1
HALLMARK_PROTEIN_SECRETION	-1.345E+00	2.909E-02	GNAS
HALLMARK_PROTEIN_SECRETION	-1.345E+00	2.909E-02	TOM1L1
HALLMARK_PROTEIN_SECRETION	-1.345E+00	2.909E-02	BET1
HALLMARK_PROTEIN_SECRETION	-1.345E+00	2.909E-02	ARFGAP3
HALLMARK_PROTEIN_SECRETION	-1.345E+00	2.909E-02	RER1
HALLMARK_PROTEIN_SECRETION	-1.345E+00	2.909E-02	SCAMP3
HALLMARK_PROTEIN_SECRETION	-1.345E+00	2.909E-02	TMED2
HALLMARK_PROTEIN_SECRETION	-1.345E+00	2.909E-02	COPE
HALLMARK_PROTEIN_SECRETION	-1.345E+00	2.909E-02	NAPA
HALLMARK_PROTEIN_SECRETION	-1.345E+00	2.909E-02	KRT18
HALLMARK_PROTEIN_SECRETION	-1.345E+00	2.909E-02	TPD52
HALLMARK_PROTEIN_SECRETION	-1.345E+00	2.909E-02	TSG101
HALLMARK_PROTEIN_SECRETION	-1.345E+00	2.909E-02	ARF1
HALLMARK_PROTEIN_SECRETION	-1.345E+00	2.909E-02	BNIP3
HALLMARK_PROTEIN_SECRETION	-1.345E+00	2.909E-02	ICA1
HALLMARK_PEROXISOME	-1.236E+00	6.197E-02	CADM1
HALLMARK_PEROXISOME	-1.236E+00	6.197E-02	CRAT
HALLMARK_PEROXISOME	-1.236E+00	6.197E-02	ACSL1
HALLMARK_PEROXISOME	-1.236E+00	6.197E-02	ERCC3
HALLMARK_PEROXISOME	-1.236E+00	6.197E-02	CTBP1
HALLMARK_PEROXISOME	-1.236E+00	6.197E-02	SLC23A2
HALLMARK_PEROXISOME	-1.236E+00	6.197E-02	PRDX5
HALLMARK_PEROXISOME	-1.236E+00	6.197E-02	LONP2
HALLMARK_PEROXISOME	-1.236E+00	6.197E-02	RETSAT
HALLMARK_PEROXISOME	-1.236E+00	6.197E-02	IDH1
HALLMARK_PEROXISOME	-1.236E+00	6.197E-02	CLN6
HALLMARK_PEROXISOME	-1.236E+00	6.197E-02	HMGCL
HALLMARK_PEROXISOME	-1.236E+00	6.197E-02	EPHX2
HALLMARK_PEROXISOME	-1.236E+00	6.197E-02	SMARCC1
HALLMARK_PEROXISOME	-1.236E+00	6.197E-02	FDPS
HALLMARK_PEROXISOME	-1.236E+00	6.197E-02	TTR

HALLMARK_PEROXISOME	-1.236E+00	6.197E-02	SOD1
HALLMARK_PEROXISOME	-1.236E+00	6.197E-02	IDI1
HALLMARK_PEROXISOME	-1.236E+00	6.197E-02	TSPO
HALLMARK_PEROXISOME	-1.236E+00	6.197E-02	PABPC1
HALLMARK_PEROXISOME	-1.236E+00	6.197E-02	PEX13
HALLMARK_PEROXISOME	-1.236E+00	6.197E-02	PEX11B
HALLMARK_PEROXISOME	-1.236E+00	6.197E-02	PEX11A
HALLMARK_PEROXISOME	-1.236E+00	6.197E-02	HRAS
HALLMARK_PEROXISOME	-1.236E+00	6.197E-02	ALDH9A1
HALLMARK_PEROXISOME	-1.236E+00	6.197E-02	SLC35B2
HALLMARK_PEROXISOME	-1.236E+00	6.197E-02	DHCR24
HALLMARK_PEROXISOME	-1.236E+00	6.197E-02	ERCC1
HALLMARK_PEROXISOME	-1.236E+00	6.197E-02	PEX6
HALLMARK_PEROXISOME	-1.236E+00	6.197E-02	ALB
HALLMARK_PEROXISOME	-1.236E+00	6.197E-02	ACOX1
HALLMARK_PEROXISOME	-1.236E+00	6.197E-02	FIS1
HALLMARK_PEROXISOME	-1.236E+00	6.197E-02	ACAA1
HALLMARK_PEROXISOME	-1.236E+00	6.197E-02	CDK7
HALLMARK_PEROXISOME	-1.236E+00	6.197E-02	CNBP
HALLMARK_PEROXISOME	-1.236E+00	6.197E-02	GNPAT
HALLMARK_PEROXISOME	-1.236E+00	6.197E-02	SLC27A2
HALLMARK_PEROXISOME	-1.236E+00	6.197E-02	ELOVL5
HALLMARK_PEROXISOME	-1.236E+00	6.197E-02	RDH11
HALLMARK_PEROXISOME	-1.236E+00	6.197E-02	SCP2
HALLMARK_PEROXISOME	-1.236E+00	6.197E-02	ACOT8
HALLMARK_PEROXISOME	-1.236E+00	6.197E-02	ECH1
HALLMARK_PEROXISOME	-1.236E+00	6.197E-02	NUDT19
HALLMARK_PEROXISOME	-1.236E+00	6.197E-02	SLC25A17
HALLMARK_CHOLESTEROL_HOMEOSTASIS	-1.261E+00	1.015E-01	PMVK
HALLMARK_CHOLESTEROL_HOMEOSTASIS	-1.261E+00	1.015E-01	FDPS
HALLMARK_CHOLESTEROL_HOMEOSTASIS	-1.261E+00	1.015E-01	CYP51A1
HALLMARK_CHOLESTEROL_HOMEOSTASIS	-1.261E+00	1.015E-01	ETHE1
HALLMARK_CHOLESTEROL_HOMEOSTASIS	-1.261E+00	1.015E-01	EBP
HALLMARK_CHOLESTEROL_HOMEOSTASIS	-1.261E+00	1.015E-01	STX5
HALLMARK_CHOLESTEROL_HOMEOSTASIS	-1.261E+00	1.015E-01	MAL2
HALLMARK_CHOLESTEROL_HOMEOSTASIS	-1.261E+00	1.015E-01	IDI1
HALLMARK_CHOLESTEROL_HOMEOSTASIS	-1.261E+00	1.015E-01	SQLE
HALLMARK_CHOLESTEROL_HOMEOSTASIS	-1.261E+00	1.015E-01	GNAI1
HALLMARK_CHOLESTEROL_HOMEOSTASIS	-1.261E+00	1.015E-01	ATF5
HALLMARK_CHOLESTEROL_HOMEOSTASIS	-1.261E+00	1.015E-01	SCD
HALLMARK_CHOLESTEROL_HOMEOSTASIS	-1.261E+00	1.015E-01	ATXN2
HALLMARK_CHOLESTEROL_HOMEOSTASIS	-1.261E+00	1.015E-01	CBS
HALLMARK_CHOLESTEROL_HOMEOSTASIS	-1.261E+00	1.015E-01	MVK
HALLMARK_CHOLESTEROL_HOMEOSTASIS	-1.261E+00	1.015E-01	HMGCR
HALLMARK_CHOLESTEROL_HOMEOSTASIS	-1.261E+00	1.015E-01	LSS
HALLMARK_CHOLESTEROL_HOMEOSTASIS	-1.261E+00	1.015E-01	PCYT2
HALLMARK_CHOLESTEROL_HOMEOSTASIS	-1.261E+00	1.015E-01	CHKA
HALLMARK_CHOLESTEROL_HOMEOSTASIS	-1.261E+00	1.015E-01	ACAT2
HALLMARK_CHOLESTEROL_HOMEOSTASIS	-1.261E+00	1.015E-01	TP53INP1

HALLMARK_CHOLESTEROL_HOMEOSTASIS	-1.261E+00	1.015E-01	SREBF2
HALLMARK_CHOLESTEROL_HOMEOSTASIS	-1.261E+00	1.015E-01	TM7SF2
HALLMARK_CHOLESTEROL_HOMEOSTASIS	-1.261E+00	1.015E-01	TRIB3
HALLMARK_CHOLESTEROL_HOMEOSTASIS	-1.261E+00	1.015E-01	FASN
HALLMARK_CHOLESTEROL_HOMEOSTASIS	-1.261E+00	1.015E-01	TMEM97
HALLMARK_CHOLESTEROL_HOMEOSTASIS	-1.261E+00	1.015E-01	ECH1
HALLMARK_CHOLESTEROL_HOMEOSTASIS	-1.261E+00	1.015E-01	DHCR7